Journal of Power Sources 265 (2014) 317–324

Contents lists available at ScienceDirect

Journal of Power Sources

journal homepage: www.elsevier.com/locate/jpowsour

Increasing the energy density of the non-aqueous vanadium redox flow battery with the acetonitrile-1,3-dioxolane–dimethyl sulfoxide solvent mixture

T. Herr*, P. Fischer, J. Tübke, K. Pinkwart, P. Elsner

Fraunhofer Institute for Chemical Technology, Joseph-von-Fraunhofer-Str. 7, DE-76327 Pfinztal, Germany

HIGHLIGHTS

- An appropriate mixture for $V(acac)_3$ was created.
- Solubility of $V(acac)_3$ could be increased up to 1.1 M.
- Discharge power density of 0.25 mW cm^{-2} could be achieved.

ARTICLE INFO

Article history:
Received 4 December 2013
Received in revised form
18 March 2014
Accepted 25 April 2014
Available online 9 May 2014

Keywords:
Vanadium acetylacetonate
Single-metal redox flow battery
Non-aqueous solvent mixtures
Energy storage
Cyclic voltammetry

ABSTRACT

Different solvent mixtures were investigated for non-aqueous vanadium acetylacetonate ($V(acac)_3$) redox flow batteries with tetrabutylammonium hexafluorophosphate as the supporting electrolyte. The aim of this study was to increase the energy density of the non-aqueous redox flow battery. A mixture of acetonitrile, dimethyl sulfoxide and 1-3-dioxolane nearly doubles the solubility of the active species. The proposed electrolyte system was characterized by Raman and FT-IR spectroscopy, cyclic voltammetry, electrochemical impedance spectroscopy and charge–discharge set-up. Spectroscopic methods were applied to understand the interactions between the solvents used and their impact on the solubility. The potential difference between oxidation and reduction of $V(acac)_3$ measured by cyclic voltammetry was about 2.2 V. Impedance spectroscopy showed an electrolyte resistance of about 2400 Ω cm^2. Experiments in a charge–discharge test cell achieved coulombic and energy efficiencies of ~95% and ~27% respectively. The highest discharge power density was 0.25 mW cm^{-2}.

1. Introduction

Redox flow batteries (RFBs) are promising energy storage systems. The energy in RFBs is stored in two electrolyte solutions, in which electroactive species are dissolved. These electrolytes are stored in separate tanks and are pumped through the battery cell, which is divided by an ion-exchange membrane. This membrane prevents undesirable ion crossover. Two advantages of an RFB are the almost infinite lifetime of the active species and the independent scalability of power and energy, thus resulting in flexible and application-oriented design of the battery.

Existing commercial RFB systems are usually based on vanadium salts dissolved in aqueous electrolytes. A good overview of redox flow batteries is given by different authors [1]. The literature outlines aqueous RFBs such as: bromine–polysulfide, iron–chromium, all-vanadium, zinc–bromine, zinc–cerium and vanadium–bromine. Most of these systems suffer from cross-contamination because of the membrane permeability, which leads to electrolyte degradation and capacity losses. Another problem of the aqueous systems is the cell potential, which is limited by the water electrolysis. Compared to aqueous systems non-aqueous systems provide wider potential windows as well as a wider temperature range due to the physical and chemical properties of the non-aqueous electrolytes [2]. Most of the non-aqueous redox flow batteries developed so far consist of unique active species in both half cells: e.g. $V(acac)_3$, $Cr(acac)_3$, $Mn(acac)_3$, $Ru(acac)_3$ etc. [1,3], which minimize capacity losses through cross-contamination. However, the main problem of non-aqueous RFBs is the low solubility of their organic electroactive species.

According to several research studies and publications it is possible to increase the solubility of redox active species by using a mixture of different solvents [4]. In this case, a phenomenon known

* Corresponding author. Tel.: +49 721 4640 503; fax: +49 721 4640 111.
E-mail address: tatjana.herr@ict.fraunhofer.de (T. Herr).

http://dx.doi.org/10.1016/j.jpowsour.2014.04.141
0378-7753/

as preferential solvation occurs. It can be used to explain how the interactions between different solvents can affect the solute–solvent interactions, and has been studied by various research groups [5]. Additionally, the solvent mixture approach has been successfully used in other storage systems like lithium-ion batteries, for example where high ionic conductivities and high chemical and electrochemical stabilities of the electrolyte solution are required [6a]. For energy storage systems like redox flow batteries this approach can provide better performance as well as an increase in the energy density due to a better solubility of the active species.

This paper reports electrochemical studies of the vanadium(III) acetylacetonate ($V(acac)_3$) active species, supported by tetrabutylammonium hexafluorophosphate ($TBAPF_6$) in a ternary solvent mixture consisting of acetonitrile (AN), 1,3-dioxolane (1,3-DO) and dimethyl sulfoxide (DMSO).

2. Experimental

2.1. Electrolytes

Electrolyte solutions were prepared by dissolving $V(acac)_3$ (97%, Aldrich) in different solvents or solvent mixtures consisting of: acetonitrile (99.8%, anhydrous, Aldrich), 1,3-dioxolane (99.8%, anhydrous, Aldrich), dimethyl sulfoxide (SeccoSolv®, anhydrous, Merck) propylene carbonate (selectipur, anhydrous, Merck), γ-butyrolactone (99%, Aldrich), *N*,*N*-dimethylformamide (99.8%, anhydrous, Aldrich), dimethoxyethane (99.5%, anhydrous, Aldrich), methylacetate (99.5%, anhydrous, Aldrich), ethylacetate (99.8%, anhydrous, Aldrich), *N*,*N*′-dimethyl propylene urea (99.0%, anhydrous, Aldrich) and dimethyl carbonate (99%, anhydrous, Aldrich). $TBAPF_6$ (≥99.0%, Aldrich) was used as supporting electrolyte.

2.2. Cyclic voltammetry experiments

Cyclic voltammetry was performed using the VC-2 voltammetry cell from ALS Co., Tokyo, Japan. A glassy carbon disc electrode (ALS Co., Tokyo, Japan) with a surface area of 0.07 cm^2 was used as a working electrode, a Pt disc electrode (ALS Co., Tokyo, Japan) as a counter electrode and a non-aqueous $Ag/AgCrypt^+$ electrode as a reference electrode, described in Ref. [8]. The reference electrode consisted of 0.005 M Ag^+ and 0.01 M Cryptand 22 (1,4,10,13-Tetraoxa-7,16-diazacyclooctadecane, 96%, Aldrich) in the electrolyte used for the measurement. Cathodic and anodic processes in the $V(acac)_3$ solution were studied in separate experiments to determine diffusion coefficients. All measurements were carried out in a glove box under argon atmosphere. Analyses were carried out at room temperature with various scan rates between 10 and 100 mV s^{-1} using a potentiostat (Ivium Compactstat, Ivium Technologies B.V., Netherlands). The concentrations of $V(acac)_3$ and $TBAPF_6$ were 0.005 M and 0.05 M respectively.

2.3. Charge–discharge experiments

For the charge–discharge experiments a test cell assembly, with both half cells separated by a Neosepta AHA anion-exchange membrane (Astom, Japan), described in Ref. [7] was used. Prior to each experiment, the membrane was pre-conditioned by soaking it in a solution containing $TBAPF_6$ in used solvent for more than 22 h. The graphite bipolar plates (FU-4369, Schunk Kohlenstofftechnik, Germany) and graphite felts (GFA 5, SGL Carbon, Germany) had a geometric area of 40 cm^2. Before introducing the electrolyte, nitrogen was purged through the cell. In both half cells an electrolyte volume of 60 ml was provided. The cycle experiment was carried out between 0.3 and 2.5 V. For each current density 6 cycles were performed. Ismatec RegloDigital tubing pump (IDEX Health & Science, Germany) was used to pump the electrolyte through the cell. The flow rate was about 25 ml min^{-1}. The concentrations of $V(acac)_3$ and $TBAPF_6$ were 0.05 M and 0.1 M respectively. ModuLab (Solartron Analytical, USA) was used as a measuring system.

2.4. Impedance experiments

Impedance measurements were performed in the test cell described above in the frequency range from 1 MHz to 10 mHz, vs. OCV at a discharged state and 10 mV amplitude with a ModuLab potentiostat (2087A/2055 A FRA Solartron Analytical, USA).

2.5. Conductivity measurements

Conductivity was measured using a Seven Easy™ Conductivity meter S30 with an InLab®731 conductivity cell (Mettler Toledo, Germany) at room temperature. The electrolyte solutions consisted of 0.01 M $V(acac)_3$ or 0.01 M $TBAPF_6$.

2.6. Viscosity measurements

Viscosity measurements were carried out with a rheometer "Physica MCR" (MCR-Modular Compact Rheometer) from the company Anton Paar GmbH, Graz, Austria. The set-up used contained a horizontal plate with 50 mm diameter and a shallow cone. The angle between the surface of the cone and the plate was approx. 1°.

2.7. Spectroscopic measurements

Raman spectra were obtained with a HORIBA LabRAM HR (JOBIN YVON Technology GmbH, Germany) at room temperature. All the spectra were recorded, employing the 532 nm exciting line of the Nd:YAG doubled laser and a CCD detector (at −70 °C). The samples were inserted into 5 mm diameter tubes. FT-IR absorbance spectra were recorded with an Equinox 55 FT-IR instrument (Bruker, Germany) with a resolution of 4 cm^{-1} and NaCl windows in a frequency range of 4000 − 400 cm^{-1}.

Different samples of AN:DMSO ratios, saturated with $V(acac)_3$, were prepared in the glove box.

2.8. Solubility measurements

Solubility was determined by incremental addition of the active species to a fixed volume of solvent in a glass flask with a stopper. Each addition of substance was followed by shaking and shelving overnight.

3. Results & discussion

3.1. Solvent–solvent interactions

As was mentioned in the introduction, solvent mixtures may differ in their solvation properties compared to pure solvents and this can influence the solubility of the active species. To create an appropriate solvent mixture the properties which cause the greatest deviations from the ideal behaviour should be found. Table 1 shows an overview of the investigated solvents: propylene carbonate (PC), dimethyl sulfoxide (DMSO), γ-butyrolactone (GBL), acetonitrile (AN), dimethylformamide (DMF), 1,3-dioxolane (1,3-DO), dimethoxyethane (DME), methylacetate (MA) and ethylacetate (EA) as well as some chosen parameters which might influence the solubility: permittivity ε, viscosity η, polarizability π^* as well as the donor and acceptor numbers. The most important parameters for the dissolving process, which induce the solubility, are the donor–acceptor properties and the polarizability, π^*, of the solvent's components [4b].

Table 1
Physical properties of organic solvents [4b,9].

	Solubility [$V(acac)_3$][a]	Solubility [$TBAPF_6$][a]	ε	η [cP]	DN [kcal mol^{-1}][b]	AN [kcal mol^{-1}][b]	π	κ [$\mu S\ cm^{-1}$]
PC	0.07	2.1	64.92	2.53	15.1	18.3	83	230
DMSO	<0.3	2.3	46.5	1.99	29.8	19.3	100	294
GBL	0.3	2.7	39.1	1.73	18	17.3	87	347
DMF	0.7	3.1	36.7	0.802	26.6	16	88	619
DMPU	0.2	1.9	36.12	2.93	15	42	–	178
AN	0.6	3.5	35.9	0.341_{30}	14.1	18.9	75	1335
DO	0.8	2.4	7.34	0.6	–	–	69	36
DME	0.6	0.3	7.2	0.455	23.9	10.2	53	48.3
MA	0.4	0.8	6.68	0.364	16.5	10.7	60	36.3
EA	0.3	0.07	6.02	0.426	17.1	9.3	55	11.92

[a] Solubility measured in mol per litre solvent.
[b] DN – donor number; AN – acceptor number.

Table 2
Solubility of $V(acac)_3$ in different solvent mixtures.

Mixture no	AN	DME	MA	DMSO	DMPU	DMF	1,3-DO	PC	GBL	c [mol $l^{-1}_{solvent}$]
1	100									0.60
2	76.2	19.0		4.8						0.75
3	0.00						100			0.80
4	89.0		5.5	5.5						0.85
5	94.1			5.9						0.90
6	94.1				5.9					0.90
7	94.1					5.9				1.00
8	76.2			4.8			19.0			1.10
9	94.1							5.9		<0.6
10	94.1								5.9	<0.6

Ratios of solvents in vol%.

Solubility tests with vanadium acetylacetonate were performed with different binary as well as ternary mixtures. In the solubility tests with the vanadium complex (Table 2) it was observed that the highest solubility was achieved in solvent mixtures, where at least one solvent has a high donor number or high polarizability, like DMSO. As can be seen from Table 2 an addition of ~6% DMSO or DMF to AN almost doubles the solubility of $V(acac)_3$. Various researchers have stated in their papers that due to the high donor and acceptor numbers of DMSO, this solvent interacts preferentially with dissolved species [5d,5e].

Fig. 1 shows the results of solubility tests of $V(acac)_3$ in different mixtures of acetonitrile and dimethyl sulfoxide. The solubility increased significantly when only a small amount of DMSO was added, and then decreased with further addition of DMSO. Similar results were achieved when measuring the conductivity of $V(acac)_3$ in different solvent mixtures (Fig. 1, circles). One explanation for this phenomenon is the structural change within the solvent mixture. The addition of DMSO distorts the association of the AN and DMSO molecules, as is described in detail in Refs. [5c,f]. These changes can be observed in the SO and CN vibrations in appropriate regions of the spectrum. It can be seen that both bands shift to lower wave numbers when more DMSO is added. A maximum shift of 10 cm^{-1} is observed for the S=O band at 1048 cm^{-1}. Fig. 2 shows the way the band changed. The corresponding band at ~1058 cm^{-1} can be attributed to a soluted DMSO molecule, while the band at 1048 cm^{-1} results from the associated DMSO molecule in the pure solvent [10]. The shift to higher wave numbers therefore indicates continuous distortion of the associated DMSO molecules. It can be also seen that up to addition of 20 vol% of DMSO to AN no shift of the band position occurs. This indicates that up to this relation DMSO interacts preferentially with AN and no DMSO aggregates are present in the solution. If more than 20 vol% DMSO is added to the solution, IR spectra show a linear relationship between the peak shift and the volume fraction, indicating DMSO aggregates are formed with higher DMSO ratio.

In order to study the influence of the solvent mixture on its interaction with $V(acac)_3$, thus on the solubility, IR spectra were obtained. The IR spectrum of different AN–DMSO solvent mixtures saturated with $V(acac)_3$ showed two bands of $V(acac)_3$ which did not overlap with the solvent bands. The first band at 1526 cm^{-1} corresponds to the conjugated C=C=C stretching vibrations (CCC-bond) and the second one at 1562 cm^{-1} to the conjugated C=O stretching vibrations [11]. The band shift to lower wave numbers was observed for the first band at 1526 cm^{-1}. Fig. 3 shows the way the band changed. It can be seen that the biggest shift to lower wave numbers occurred when only 5% of DMSO was added to AN. The shift to lower wave numbers indicates a decrease of the CCC binding energy. This can be explained by a stronger interaction of the CCC-bond with dissolved DMSO molecules. The DMSO

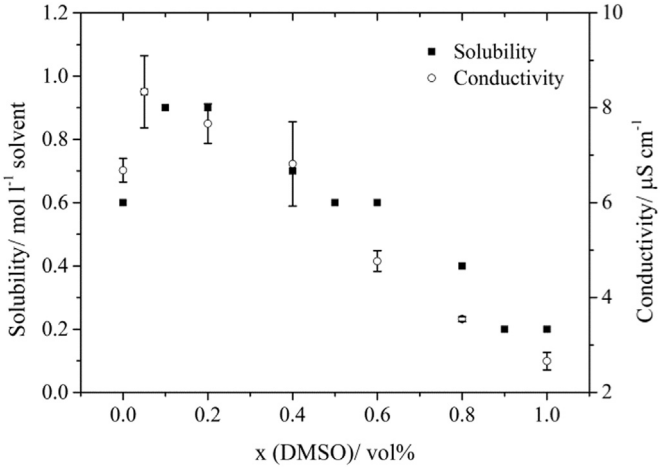

Fig. 1. Solubility and conductivity results of $V(acac)_3$ in different AN/DMSO mixtures (0.01 M $V(acac)_3$ for conductivity measurements).

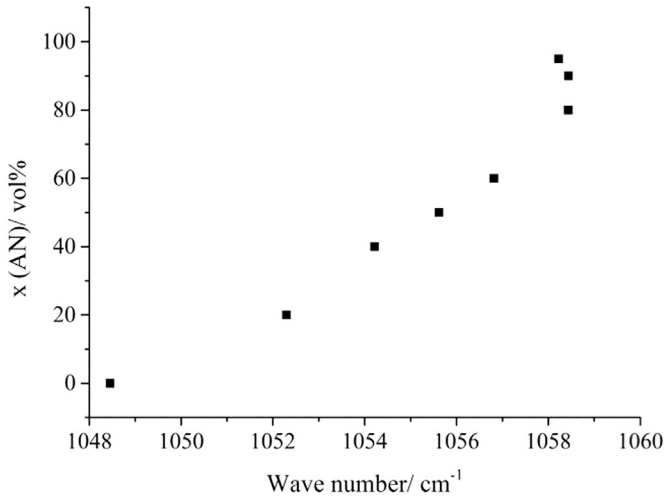

Fig. 2. Spectral parameters of the SO band at 1045 cm^{-1} in binary AN/DMSO mixtures.

molecule exhibits higher donor ability to the partially positive charged CCC-bond compared to the AN molecule of the pure solvent. This is in accordance with the previous statement about a preferential solvation of $V(acac)_3$ by DMSO.

The preferential solvation also influences the mobility of the $V(acac)_3$ complex, as can be seen in the increased conductivity (Fig. 1). Nevertheless, if the ratio of DMSO is increased the conductivity decreases. The high viscosity of DMSO leads then to lower mobility of the $V(acac)_3$ and therefore to lower conductivities. These results correspond well to the simulations of E. Bernardi and H. Stassen [5f]. They simulated the diffusion coefficients for DMSO–AN mixtures and calculated that the highest D is achieved when only a small amount of DMSO is added.

In summary, small quantities of DMSO significantly improve the solubility and the conductivity of $V(acac)_3$ in AN. For a non-aqueous electrolyte with increased energy density, the solution mixture should therefore contain both solvents.

3.2. Conductivity of solvent mixtures

To obtain high energy efficiencies and discharge power densities of the flow battery, the high conductivity (conductance, κ) of the electrolyte is also an important value.

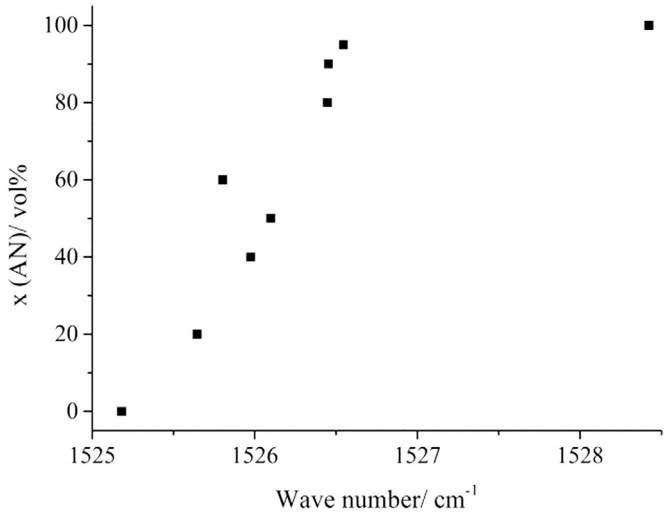

Fig. 3. Spectral parameters of CCC conjugation bond of $V(acac)_3$ in different AN/DMSO mixtures.

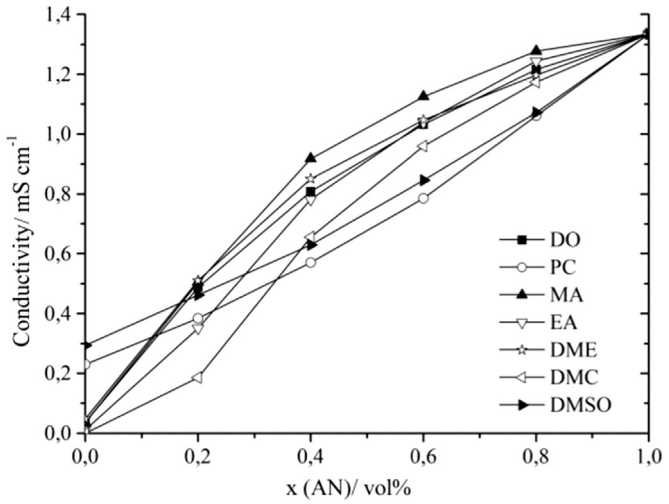

Fig. 4. Conductivity measurements in different binary solvent mixtures with 0.01 M $TBAPF_6$.

The conductivity (conductance) measurements in pure solvents with $TBAPF_6$ as a supporting electrolyte are shown in Table 1. It can be seen that the conductivity in AN is more than two times higher than in DMF and 4 times higher than in DMSO. Conductivity measurements in mixed solvents (Fig. 4) showed that the amount of AN in the solvent mixture should be kept high to maintain a high conductivity in the solution.

Fig. 5 shows the $1/\kappa$ (resistance) and η as a function of the composition of AN with a highly viscous solvent as DMSO, which should be present in the mixture. It can be seen that the conductivity of the AN/DMSO mixture is proportional to its viscosity (Equations (5) and (6)). The viscosity of the solvents therefore also plays an important role in terms of a high conductivity, and can influence the conductivity even more than the permittivity of the solvent [6]. According to this result, the amount of DMSO should be kept as low as possible to maintain high conductivity.

$$\kappa = \sum(z_i F u_i c_i) = \sum \lambda_i c_i \tag{5}$$

$$u^{+} = (z e_0 E)/6\pi\eta_{el} r_{Cation} \tag{6}$$

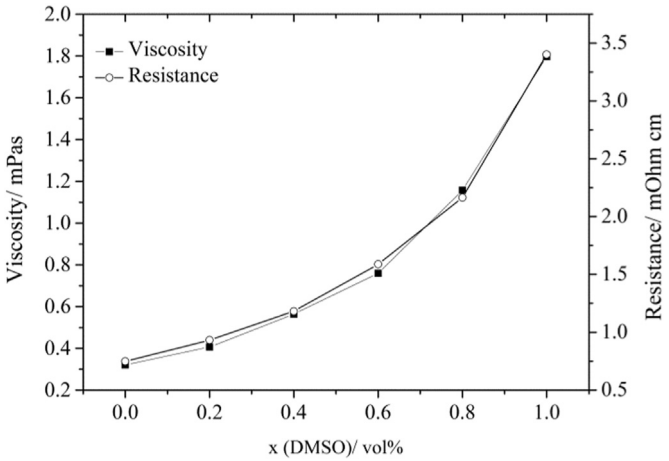

Fig. 5. Viscosity and ohmic resistance vs. DMSO content in the AN/DMSO mixture.

where u_i is the ion mobility, F is the Faraday constant, c_i, z_i and λ_i – concentration, charge and the ionic (molar) conductivity of the ion i, e_0 – elementary charge, E – field strength, r_{cation} – radius of solvated cations and η viscosity.

This consideration corresponds to the results of the solubility measurements with $V(acac)_3$, where only small amounts of DMSO significantly change solubility.

Additional parameters which influence the conductivity are [6a]:

- The radii of the ions
- The association constant of the salt
- The role of selective solvation
- The competition of solvation and association

To summarize the results outlined above, the following criteria should be fulfilled to obtain a high solubility of the redox active species and a high conductivity of the electrolyte solution:

- High amount of acetonitrile
- One solvent with a high donor number and polarizability
- Viscosity should be kept as low as possible

With these criteria for an electrolyte solution, a RFB cell with high energy density and discharge power density can be prepared. The most promising solvent mixture is mixture No. 8 (ADD mixture), Table 2. This mixture contains 76.2 vol% acetonitrile and 4.8 vol% DMSO, and the remainder up to 100% was filled with 1,3-DO, because the solubility could be increased further. By contrast Raman spectrum showed no changes when 1,3-DO was added to the AN/DMSO mixture.

The ADD mixture was used throughout this study.

3.3. Electrochemical behaviour of $V(acac)_3$ in the ADD solvent mixture

As was mentioned in the previous chapter, ADD solvent (Table 2) enables the highest solubility of $V(acac)_3$, thus the highest capability for increased energy density in a redox flow battery. To evaluate reversibility and kinetics of $V(acac)_3$ redox reactions, electrochemical studies were performed.

A cyclic voltammogram of $V(acac)_3$ in the ADD-mixture is depicted in Fig. 6. It shows two characteristic redox processes associated with reactions (7) and (8).

$$V(acac)_3^+ + e^- \rightleftharpoons V(acac)_3 \quad (7)$$

$$V(acac)_3 + e^- \rightleftharpoons V(acac)_3^- \quad (8)$$

The overall reaction is:

$$V(acac)_3^+ + V(acac)_3^- \rightleftharpoons 2V(acac)_3 \quad (9)$$

The cell potential between the cathodic (8) and anodic (7) reaction of the system is 2.2 V. Within this potential window no other electrochemical reactions take place. Both peaks show quasi-reversible behaviour according to the criteria for a reversible redox process [12].

The peak separation ΔE of the reduction and oxidation processes of $V(acac)_3$ are 118 mV and 126 mV respectively at 50 mV s^{-1}. The observed change in peak separation with a scan rate from 10 to 100 mV s^{-1} was 39 mV for the oxidation and 45 mV for the reduction process. The increase of ΔE with scan rate could be due to uncompensated ohmic resistance between the reference and working electrodes [13], as the solution conductance is not high enough.

The values of the peak current ratios, j_{pa}/j_{pc}, indicate a reversible behaviour. These are in most cases near unity.

The relationship between the peak current and the square root of the voltage scan rate, which is described by the Randles–Sevcik equation (10), should show a linear behaviour.

$$i_p = 2.69 \cdot 10^5 n^{3/2} A c D^{1/2} v^{1/2} \quad (10)$$

Here n is the number of transferred electrons in the reaction ($n = 1$), A the electrode area (0.07 cm^2), c the concentration of active species in the bulk solution (0.005 M), D the diffusion coefficient of the active species and v the scan rate. For both reactions a linear behaviour with a correlation coefficient of 0.999 is observed (Fig. 7), indicating a diffusion controlled electron transfer at the scan rates used. The non-zero intersection with the y-axis is explained in terms of the disproportionation reaction of $V(acac)_3$. In this case all three species are present at the equilibrium at low scan rates [14]. The use of an undivided CV-cell consequently enables an almost constant concentration of the active species at low scan rates.

Additionally, the reaction rate constant provides information about the type of reaction. To calculate the rate constant, the Nicholson's equation (11) [15] and estimated values of Ψ using $\alpha = 0.5$ were used:

$$\psi = \gamma^{\alpha} k_s \Big/ (\pi a D_O)^{1/2} \quad (11)$$

$$\gamma = (D_O/D_R)^{1/2} \quad (12)$$

$$a = nFv/RT \quad (13)$$

For the peak differences of 126 mV and 118 mV, respective Ψ-values of 0.32 and 0.38 were used. Thus the values of rate constants for the reduction and oxidation processes are found to be 1.97×10^{-3} cm s^{-1} and 2.44×10^{-3} cm s^{-1}, respectively, which are in the range of a quasi-reversible transfer reaction [12b]. Compared to the aqueous vanadium system these values are higher by a factor of ten, thus indicating faster kinetics (Table 3).

If a wider potential window is considered, an additional peak at ~1.2 V could be observed (Fig. 6). This reaction is attributed to the formation of vanadyl acetylacetonate ($VO(acac)_2$). $VO(acac)_2$ is mostly formed in presence of water residues [3a,e,h].

To elucidate the reaction kinetics, the Nicholson–Shain criterion (the variation of the current function, (i_{pc}/v), with the scan rate v),

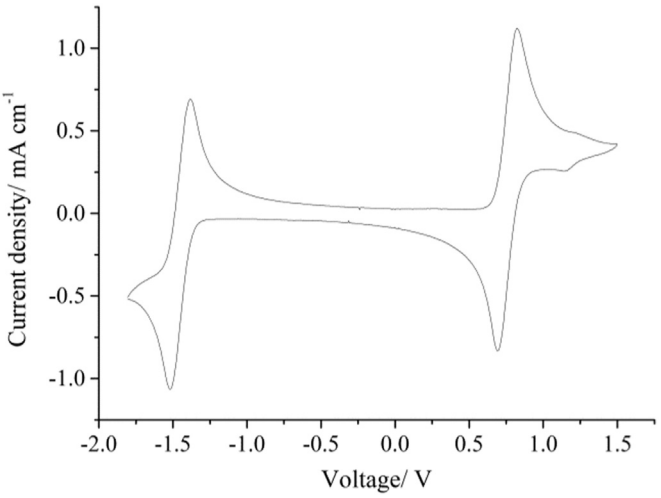

Fig. 6. Cyclic voltammograms of 0.005 M $V(acac)_3$ and 0.05 M $TBAPF_6$ in ADD-mixture, 100 mV s^{-1}, glassy carbon electrode (0.07 cm^2) vs. $AgCrypt^+$ reference electrode.

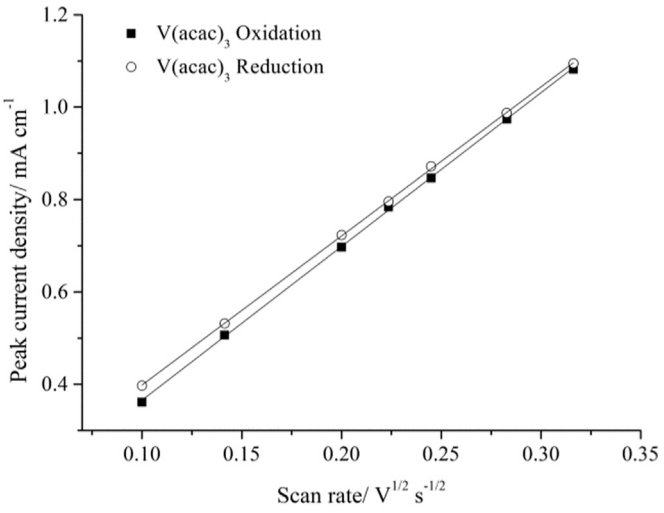

Fig. 7. Variation of peak current density (j_p) with square root of scan rate for $V(acac)_3$ redox couples in cyclic voltammetry experiments carried out in ADD-mixture.

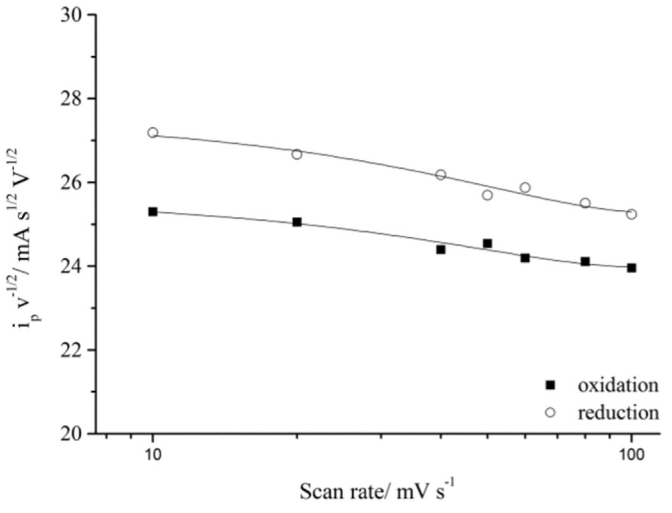

Fig. 8. Plots of $i_p/\nu^{0.5}$ vs. ν for oxidation and reduction of $V(acac)_3$ in ADD-mixture.

was applied. The results are shown in Fig. 8. The current functions decrease slightly in parallel to each other with scan rate, indicating a similar reaction mechanism. Nicholson–Shain criteria state that such behaviour indicates a charge transfer followed by an irreversible chemical reaction. This is in accordance with the previously-mentioned formation of $VO(acac)_2$ through a chemical reaction of $V(acac)_3$ and water.

Diffusion coefficients can be calculated from the slope of the plots due to Equation (10) for the reversible case. These are found to be $5.71 \times 10^{-6} \pm 0.18 \times 10^{-6}$ cm^2 s^{-1} for the reduction process and $6.97 \times 10^{-6} \pm 1.02 \times 10^{-6}$ cm^2 s^{-1} for the oxidation process. Diffusion coefficients for the aqueous vanadium system are in the same range (Table 3).

The overall results of cyclovoltammetric measurements can be summarized as follows: both redox reactions of $V(acac)_3$ show quasi-reversible behaviour, which nevertheless could be disturbed by $VO(acac)_2$ formation. The last fact might cause coulombic efficiency and capacity losses.

3.4. Battery tests

3.4.1. Electrochemical impedance spectroscopy measurements

To characterize the battery cell and determine the rate limiting step, electrochemical impedance spectroscopy (EIS) was applied [17]. Fig. 9 shows the results from EIS measurements at 0 V vs. OCV in the ADD-mixture.

The EIS spectrum shows a small partially-resolved semi-circlet in the high-frequency range. It is attributed to the electrolyte resistance. In solutions with a good conductivity the electrolyte capacity is negligible and the first arc is absent [17b]. In the low-frequency range a big semi-circle is observed, which is attributed to the redox-reaction of the active species.

The electrolyte resistance is about 2400 Ω cm^2. The high value is a result of the low conductivity of the electrolyte. This impedance spectrum also shows that the reaction is diffusion controlled reaction and the rate-determining step in the whole process, which is in agreement with the CV results.

3.4.2. Charge–discharge experiments

Fig. 10 shows charge–discharge curves and current density progress of the system in the ADD-mixture at three different current densities.

Fig. 10B shows the third cycle at 0.3 mA cm^{-2}. It can be seen that at the beginning of charge there was firstly a strong voltage increase up to 1.15 V, followed by a slowly increasing voltage up to 2.23 V and the main plateau up to 2.5 V. During the next OCV measurement the voltage rapidly decreased to 2.22 V after 60 s. During discharge one more step appeared. Firstly a rapid decrease down to 1.99 V was observed. After slight decrease to 1.89 V, a more rapid decrease to 0.85 V followed. The last main plateau was observed from 0.85 V to the end of discharge at 0.3 V. Additional steps during discharge could be attributed to side reactions associated with ligand oxidation [3e].

To determine the value of polarization the open-circuit voltage (OCV) was measured after each charge and discharge process over 60 s. The polarization voltage increased over the cycles. The increase in the polarization voltage (or overpotential) is probably caused by the low conductivity of the electrolyte and high membrane resistance, which is in agreement with the impedance measurements. The electrolyte resistance of the non-aqueous electrolyte is much higher compared to the aqueous all-vanadium system carried out with the same set up described in Ref. [7]. In the latter case the ohmic resistance is lower than 40 Ω cm^2, which is a factor 60 lower than in the non-aqueous RFB. High membrane resistance leads to the poor transport properties.

Mass transport limitations as well as degradation of the active material cause high capacity losses. Fig. 11 shows the capacity efficiency (Q) as a function of the applied current density. It can be seen that already after the first cycle there is a loss of about 40%. This could be caused by the side reaction of $V(acac)_3$ to $VO(acac)_2$, and by ligand oxidation. On average, there are 5% capacity losses compared to the previous cycle. Since the charge–discharge measurements are performed in air, there is no 100% elimination of traces of oxygen or water from the ambient air. This is the main reason for the $VO(acac)_2$ formation [3e].

Table 3
An overview of the physical and electrochemical data for the aqueous and non-aqueous vanadium redox flow batteries.

	Solubility [M]	k_{Ox} [cm s^{-1}]	k_{Red} [cm s^{-1}]	D_{Ox} [cm^2 s^{-1}]	D_{Red} [cm^2 s^{-1}]	CE/EE [%]	OCV [V]	Ref.
Aq. system	2	7.5×10^{-4}	1.2×10^{-4}	1.4×10^{-6}	1.5×10^{-6}	90/73	1.6	[1c,16]
Non-aq. system	~1.1	2.44×10^{-3}	1.97×10^{-3}	6.97×10^{-6}	5.71×10^{-6}	95/22	2.2	This study

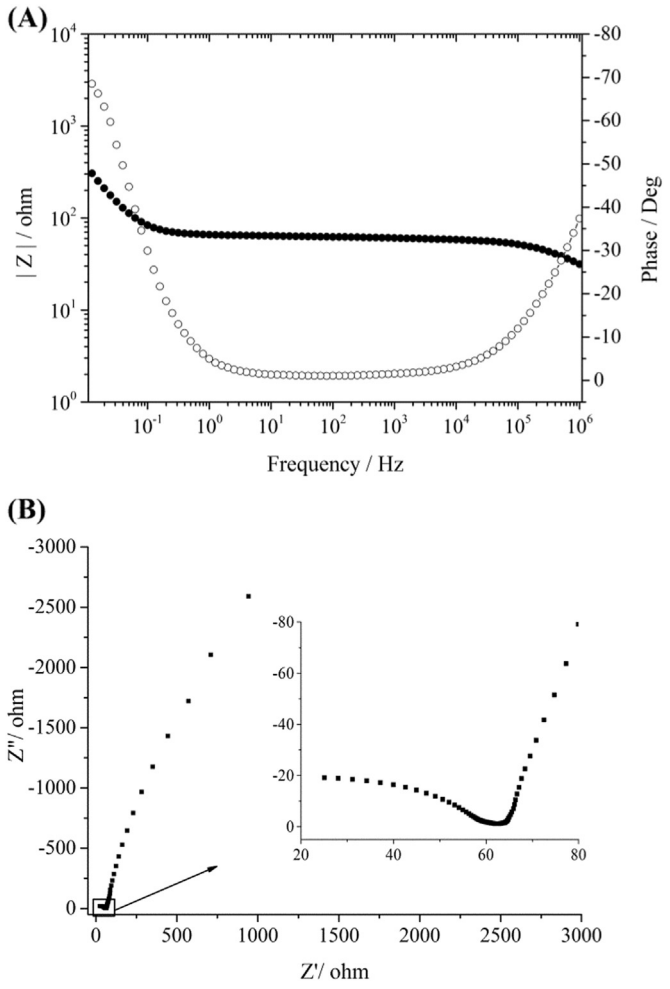

Fig. 9. (A) Bode (open circles describe the phase) and (B) Nyquist plots of 0.05 M $V(acac)_3$ with 0.1 M $TBAPF_6$ in ADD-mixture (Neosepta AHA anion exchange membrane, 0 V bias, 40 cm^2 flow cell).

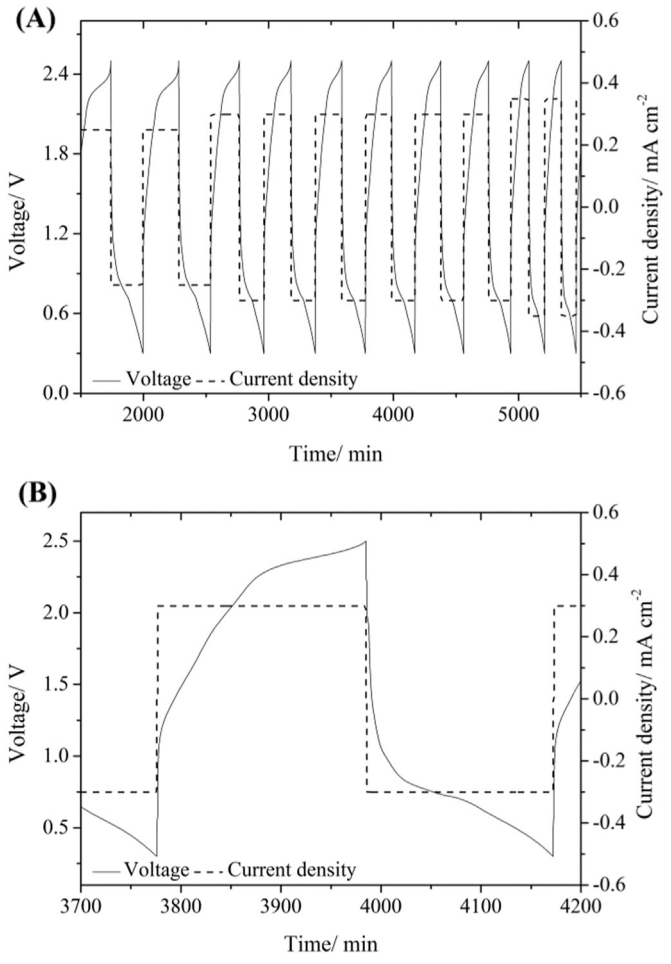

Fig. 10. A) Charge/discharge curves (solid line) and current density curves (dashed line), B) third charge/discharge cycle at 0.3 mA cm^{-2} (0.05 M $V(acac)_3$, 0.1 M $TBAPF_6$, ADD-mixture, Neosepta AHA anion exchange membrane, 40 cm^2 flow cell).

Nevertheless, at the highest current density, the highest CE of 95% (Fig. 11) could be achieved in this study, which is comparable to CE in aqueous systems (Table 3) [1]. This is in accordance with the CV results, which describe both reactions as quasi-reversible. The main reason for the 5% lower CE is cross-over through the membrane. Fig. 11 also shows the voltage efficiency (VE), energy efficiency (EE) and discharge power density as a function of the current density. It can be seen that VE and EE decrease from ~35 to 22% with increasing current density. Low voltage efficiency depends directly on the overpotentials created in the system. This also has an impact on the energy efficiency, which can be described as the product of CE and VE. It is also well known that discharge at a relatively high rate for relatively short periods of time lowers efficiencies [18].

In summary, the main reason for efficiencies as well as capacity losses is low conductivity of the electrolyte, high membrane resistance and the susceptibility of the active species to environmental effects.

4. Conclusions

A new approach in the development of a non-aqueous redox flow battery was presented within this paper. The well-known vanadium acetylacetonate redox flow battery with tetrabutylammonium hexafluorophosphate as supporting electrolyte in a solvent mixture was investigated. This new electrolyte based on a ternary solvent mixture consisting of acetonitrile, 1,3-dioxolane and dimethyl sulfoxide, nearly doubled the solubility of $V(acac)_3$.

The following important conclusions could be drawn from the studies described above:

The largest increase in solubility was attributed to the presence of DMSO as a co-solvent. Using spectroscopic methods higher solubility could be interpreted in terms of the preferential solvation of $V(acac)_3$ resulting from the small amount of DMSO added.

Electrochemical studies of the solvent mixture showed similar behaviour compared to pure acetonitrile. A cyclic voltammogram showed that the two main quasi-reversible redox couples were located 2.2 V from each other. Electrochemical impedance spectroscopy measurements showed that the charge-transfer reaction is the limiting step in the whole process. For the charge–discharge experiments a coulombic efficiency of ~95%, but a mean energy efficiency of ~27% was achieved, which was attributed to high polarization and ohmic losses. The discharge power density reached almost the highest value of 0.25 mW cm^{-2}.

All in all this means that an appropriate membrane with high conductivity and good transport properties, and an electrolyte with highly conductive support and additives for stabilization of the active species should lead to lower overpotentials, constant capacity values and high efficiencies. The high conductivity of the

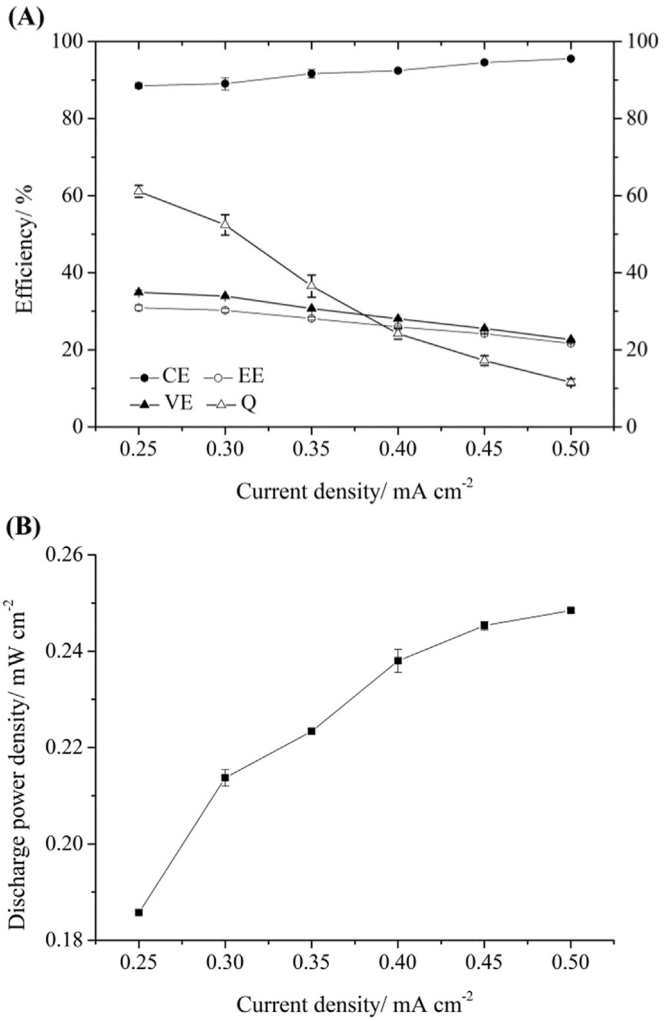

Fig. 11. CE, VE, EE, capacity (A) and discharge power density (B) vs. current density of the battery tests with $V(acac)_3$ in the ADD-mixture.

electrolyte would also positively affect the discharge power density of the system. This is the main challenge for future non-aqueous redox flow batteries.

Acknowledgements

This project was supported by the Fraunhofer-Gesellschaft, especially by the Institute for Chemical Technology.

References

[1] (a) M. Skyllas-Kazacos, M.H. Chakrabarti, S.A. Hajimolana, F.S. Mjalli, M. Saleem, J. Electrochem. Soc. 158 (2011) R55;
(b) A.Z. Weber, M.M. Mench, M. Matthew, J.P. Meyers, P.N. Ross, J.T. Gostick, Q. Liu, J. Appl. Electrochem. 41 (2011) 1137;
(c) C. Ponce de León, A. Frías-Ferrer, J. González-García, D.A. Szánto, F.C. Walsh, J. Power Sources 160 (2006) 716;
(d) P. Leung, X. Li, C. Ponce de Leon, L. Berlouis, C.T.J. Low, F.C. Walsh, RSC Adv. 2 (2012) 10125;
(e) S.-H. Shin, S.-H. Yun, S.-H. Moon, RSC Adv. 3 (2013) 9095;
(f) W. Wang, Q. Luo, B. Li, X. Wei, L. Li, Z. Yang, Adv. Funct. Mater. 23 (2013) 970.
[2] H.-J. Gores, J. Barthel, Naturwissenschaften 70 (1983) 495.
[3] (a) Q. Liu, A. Sleightholme, A. Shinkle, Y. Li, L. Thompson, Electrochem. Commun. 11 (2009) 2312;
(b) M. Chakrabarti, R. Dryfe, E. Roberts, Electrochim. Acta 52 (2007) 2189;
(c) Q. Liu, A. Shinkle, Y. Li, C. Monroe, L. Thompson, A. Sleightholme, Electrochem. Commun. 12 (2010) 1634;
(d) A. Sleightholme, A. Shinkle, Q. Liu, Y. Li, C. Monroe, L. Thompson, J. Power Sources 196 (2011) 5742;
(e) A. Shinkle, A. Sleightholme, L. Griffith, L. Thompson, C. Monroe, J. Power Sources 206 (2012) 490;
(f) W. Wang, W. Xu, L. Cosimbescu, D. Choi, L. Li, Z. Yang, Chem. Commun. 48 (2012) 6669;
(g) J. Noack, J. Tübke, K. Pinkwart, DE patent 10 2009 009 357 A1, 2010; (h) T. Herr, J. Noack, P. Fischer, J. Tübke, Electrochim. Acta 113 (2013) 127.
[4] (a) A. Schwake, Elektrolytlösungen und deren Verwendung, DE Patent 10212609A1, 2003; (b) Y. Marcus, Chem. Soc. Rev. 22 (1993) 409;
(c) H.J. Gores, J.M.G. Barthel, Pure Appl. Chem. 67 (1995) 919.
[5] (a) A. Maitra, S. Bagchi, J. Phys. Chem. B 112 (2008) 2056;
(b) A. Ben-Naim, J. Phys. Chem. 93 (1989) 3809;
(c) J. Jadzyn, J. Swiergiel, J. Phys. Chem. B 115 (2011) 6623;
(d) V. Sasirekha, et al., Spectrochim. Acta Part A 71 (2008) 766;
(e) M. Morita, F. Tachihara, Y. Matsuda, Electrochim. Acta 32 (1987) 299;
(f) E. Bernardi, H. Stassen, J. Chem. Phys. 120 (2004) 4860.
[6] (a) C. Daniel, J.O. Besenhard, Handbook of Battery Materials, second ed., Wiley-VCH Verlag GmbH & Co. KGaA, Weinheim, 2011;
(b) M.N. Roy, et al., Fluid Phase Equilib. 322–323 (2012) 159.
[7] J. Noack, J. Tuebke, ECS Trans. 25 (2010) 235.
[8] K. Izutsu, M. Ito, E. Sarai, Anal. Sci. 1 (1985) 341.
[9] (a) K. Izutsu, Electrochemistry in Nonaqueous Solutions, Wiley-VCH Verlag GmbH, Weinheim, 2002;
(b) B.J. Barker, et al., Angew. Chem. 91 (1979) 560;
(c) J. Stroka, et al., J. Solut. Chem. 19 (1990) 743;
(d) Safety Data Sheet for 1,3-Dioxolane, Novolyte Technologies, 2009.
[10] (a) W.A. Alves, P.S. Santos, J. Raman Spectrosc. 38 (2007) 1332;
(b) M.I.S. Sastry, S. Singh, J. Raman Spectrosc. 15 (1984) 80.
[11] B. Vlckova, B. Strauch, M. Horak, Collect. Czech. Chem. Commun. 52 (1987) 686.
[12] (a) R.S. Nicholson, I. Shain, Anal. Chem. 36 (1964) 706;
(b) J. Heinze, Angew. Chem. 96 (1984) 823;
(c) B. Speiser, Chem. Unserer Zeit 15 (1981) 62.
[13] R.S. Nicholson, Anal. Chem. 37 (1965) 667.
[14] A. Shinkle, A.E.S. Sleightholme, L.T. Thompson, C.W. Monroe, J. Appl. Electrochem. 41 (2011) 1191.
[15] R.S. Nicholson, Anal. Chem. 37 (1965) 1351.
[16] (a) E. Sum, M. Skyllas-Kazacos, J. Power Sources 15 (1985) 179;
(b) E. Sum, M. Rychcik, M. Skyllas-Kazacos, J. Power Sources 16 (1985) 85.
[17] (a) X.-Z. Juan, C. Song, H. Wang, J. Zhang, Electrochemical Impedance Spectroscopy: Theory, Experiment and Applications, John Wiley & Sons, Inc., Hoboken, New Jersey, 2005;
(b) P. Kurzweil, H.-J.- Fischle, J. Power Sources 127 (2004) 331.
[18] J. Eyer, G. Corey, Energy Storage for the Electricity Grid: Benefits and Market Potential Assessment Guide. Tech. Rep. SAND2010-0815, Sandia National Laboratories, February 2010.

Glossary

A: electrode surface area
AN: acetonitrile
c: bulk concentration
CE: Coulombic efficiency
CV: cyclic voltammogram
D: diffusion coefficient
DME: dimethoxyathane
DMF: dimethylformamide
DMSO: dimethyl sulfoxide
1,3-DO: 1,3-dioxolane
EA: ethylacetate
EE: energy efficiency
EIS: electrochemical impedance spectroscopy
GBL: γ-butyrolactone
Hacac: acetylacetone
j_p: peak current
MA: methylacetate
n: number of transferred electrons
OCV: open circuit voltage
PC: propylene carbonate
RFB: redox flow battery
$TBAPF_6$: tetrabutylammonium hexafluorophosphate
$V(acac)_3$: vanadium acetylacetonate
VE: voltage efficiency
ν: scan rate